Combustion and Flame 260 (2024) 113117

Contents lists available at ScienceDirect

Combustion and Flame

journal homepage: www.sciencedirect.com/journal/combustion-and-flame

Observing coalescence of aluminum nanoparticles during burning using aluminum/ammonia perchlorate sandwiched films

Haiyang Wang [1], Yujie Wang [1], Michael R. Zachariah [*]

Department of Chemical and Environmental Engineering, University of California, Riverside, CA 92521, USA

ARTICLE INFO

Keywords:
Aluminum nanoparticles
Ammonium perchlorate
Agglomerates
Flame propagation
Electrospraying deposition

ABSTRACT

To observe the agglomeration, an important parasitic process in metal composite combustion, sandwiched structures with laminates of aluminum (Al) and ammonia perchlorate (AP) layers are prepared and characterized by high-speed macro and microscopic imaging systems with pyrometry. The bilayer structure prepared by electrospraying was confirmed by Scanning Electron Microscopy/Energy Dispersive Spectroscopy (SEM/EDS) and the composition was confirmed by thermogravimetric analysis/differential thermal calorimetry (TGA/DSC). We found that the burn rate of the Al/AP sandwich films increases with the decrease of bilayer thickness of Al and AP, owing to the shorter diffusion distance between fuel and oxidizer. More importantly, the complete process of the agglomeration/sintering of Al nanoparticles (NPs) is observed *in-situ,* which demonstrates the different stages of agglomeration process of Al NPs. Temperature measurement from pyrometry reveals the temperature of agglomerates during combustion, consistent with the agglomerate size and burn rate observation. Simple calculations based on "pocket-theory" support the observed changes in agglomeration size with bilayer thickness.

1. Introduction

Aluminum (Al) particles are commonly used as additives in energetic composites such as propellants, explosives, and pyrotechnics to increase the overall energy density [1–6]. Compared to conventional Al microparticles, the nano-sized counterparts offer a higher energy release rate and much lower ignition temperature (1000 K vs 2300 K) [7–9]. However, due to the high specific surface area, nano-sized Al particles suffer from processing difficulties that limit the overall mass loading that can be achieved [10,11], as well as severe pre-combustion sintering and in-combustion agglomeration/sintering [12–14]. These effects rapidly increase the effective burning size of Al particles during combustion, lowering the burning and energy release rates, and effectively muting much of the theoretical benefits of going to the nanoscale.

The agglomeration of micro-sized aluminum (Al) particles has been commonly observed and studied in solid propellants and recent studies indicate that losses in specific impulse (two-phase loss) attributed to agglomeration may cancel out the advantages of the addition [15–17]. Such studies normally characterize the agglomerates of Al using ex-situ techniques, such as by quench/capture during burning, followed by electron-microscopic characterization [18,19]. Recently, in addition to ex-situ studies, *in-situ* techniques such as time-resolved X-ray imaging [20–22] and digital in-line holography [16,17] have been employed to obtain more detailed information about the formation process and movement of the Al agglomerates in solid propellants. High-speed microscopy and pyrometry have been found to be useful techniques to observe the agglomeration of nanosized Al particles at high spatial (μm) and temporal (μs) resolution [23–25]. In our more recent works, we were able to directly observe and engineer changes to Al agglomeration and flame propagation in composites with the addition of either reactive or non-reactive fibers [26,27]. The same technique was also used to monitor and characterize the stand-off flame distances and flame behavior from Ti/$Ca(IO_3)_2$ pyrolant composites [28].

Despite these and other efforts, the details of Al agglomerate formation at early stages are still unclear [3]. In this study, as shown in Fig. 1a, we refer to "Al aggregates" as those materials that are the starting structures of pre-ignition/combustion. Upon being heated to near the melting point of Al (933 K), the core begins to melt and diffuse into the shell, making it softer and thus enabling sintering and loss of surface area [14]. With the significant onset of the highly exothermic

* Corresponding author.
E-mail address: mrz@engr.ucr.edu (M.R. Zachariah).
[1] These authors contributed equally.

https://doi.org/10.1016/j.combustflame.2023.113117
Received 23 June 2023; Received in revised form 20 September 2023; Accepted 5 October 2023
Available online 21 December 2023

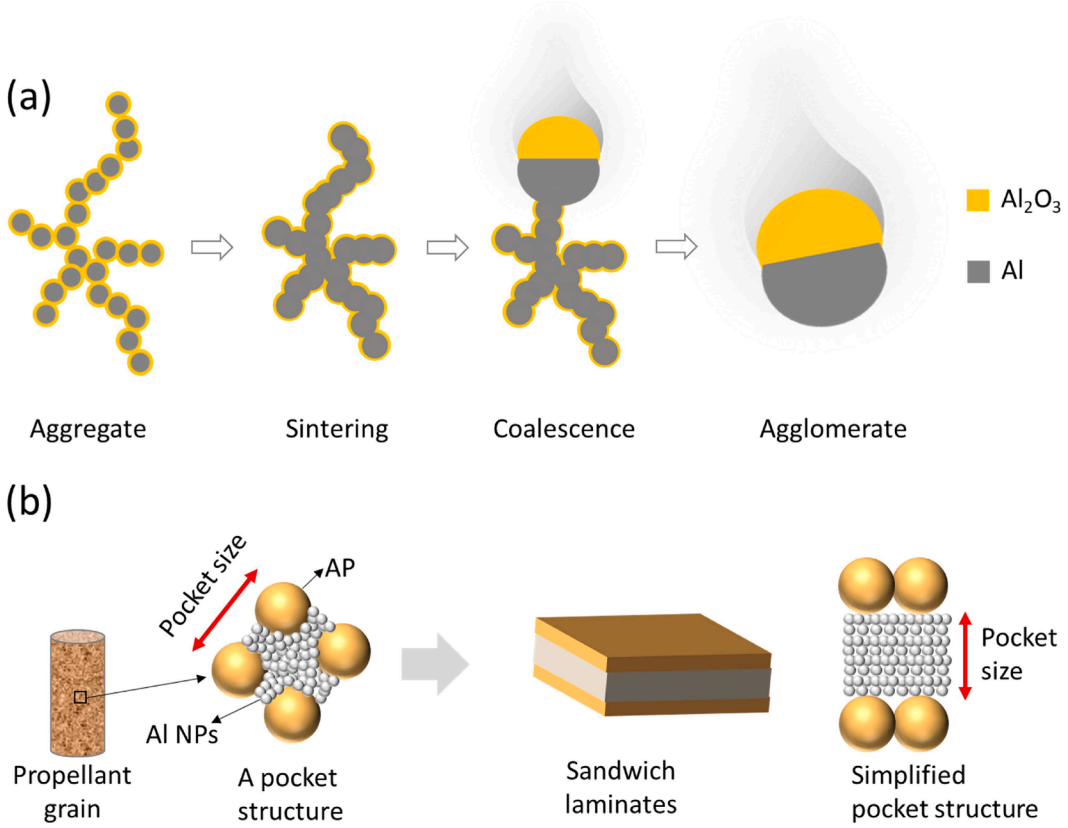

Fig. 1. Morphologies (a) at different stages of sintering/coalescence and burning. A typical "pocket" structure and simplified "pocket" structure in a solid propellant gain and sandwich laminate Al/AP in this study (b).

oxidation reaction, "sintering" is accelerated and burning results in larger droplets with evidence of phase separation between Al_2O_3 and Al. This finally leads to the well-known "snowman" droplet. The final size of the Al agglomerates (snowman structure) can be affected significantly by the size and size distribution of the oxidizer – ammonium perchlorate. Apparently, replacing conventional Al microparticles with Al NPs can also largely reduce the size of Al agglomerates. These connections between propellant microstructure and agglomerates were addressed by a "pocket" model [29–31]. As shown in Fig. 1b, A "pocket" is the volume of the fuel – Al NPs occupied, which is outlined by the oxidizer particles. Previously, we successfully engineered the size of the Al agglomerate by using different size and morphology coper oxide particles/wires to tune the "pocket" size of Al [26].

As we know, heterogeneous compositions of fuel (aluminum, Al), oxidizers (ammonium perchlorate, AP), and the binder (Hydroxyl-terminated polybutadiene, HTPB) are randomly packed in solid propellants, which at the microscopic level leads to a complex burning surface. To gain a deeper understanding of the interaction between the binder combustion and the fuel-oxidizer diffusion-reaction associated with gas/heat release, we need a more precise and controlled method for manipulating mixing and diffusion distances. To that end sandwiched structures of solid propellants with laminates of AP and HTPB have been studied. Previous studies have emphasized the importance of the leading-edge flames (LEF) between oxidizer rich layer (AP) and fuel layer (HTPB) in non-aluminized propellants, which is affected by the packing of different size AP particles [32–38]. On the other hand, morphological restructuring of the metallic fuel has not been a focus [39].

In this work, we simplified the 3D complex heterogeneous composition of Al/AP/binder with two dimensional Al/AP laminate (Fig. 1b). Nitrocellulose (NC) was chosen as the binder due to its relatively low decomposition and ignition temperature (~200 °C). The Al/AP laminate sandwich films with a total thickness of ~100 μm and different bilayer thicknesses of Al and AP are prepared by electrospray deposition. The thickness of Al layer in the sandwich laminate can be regarded as the "pocket" size of Al aggregates in a solid propellant (Fig. 1b). The films are burnt in an inert environment and characterized by both macroscopic and microscopic high-speed imaging of the combustion. We found that the burn rate of the films decreases with the increase of layer thickness, owing to the longer diffusion distance between fuel and oxidizer. More importantly, the complete process of the agglomerating of Al NPs is observed *in-situ* and the relationship between the agglomeration size and the burn rate is demonstrated. Simple calculations based on "pocket-theory" support the observed changes in agglomeration size with the layer thickness.

2. Experimental section

2.1. Materials

Aluminum nanoparticles were purchased from Argonide Corporation with an average size of ~50 nm and an active content of 67 wt% according to thermogravimetric measurement. The Collodion solution (4–8 wt% in ethanol/diethyl ether) was obtained from Sigma-Aldrich. Ethanol (200 proof) was purchased from Koptec Inc. Diethyl ether (99 %) and N, N-Dimethylformamide (DMF, 99.8 %) were purchased from Fisher Scientific. Ammonium perchlorate (AP, reagent grade, ~200 μm) was purchased from Alfa Aesar.

2.2. Precursor preparation

Nitrocellulose (NC) was obtained by drying the collodion solution (4–8 wt% in ethanol/diethyl ether) in a fume hood overnight. NC is chosen primarily due to its binding ability without much interaction

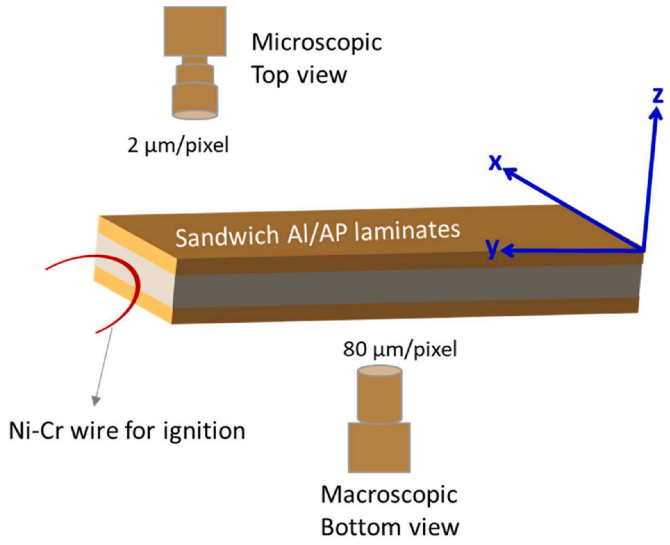

Fig. 2. Setup of macroscopic and microscopic imaging systems used in this study.

with nano-Al particles. Unlike other binder candidate such as polyvinylidene fluoride (PVDF), which will react with Al and hinder the agglomerating process [24–28]. NC has low decomposition and ignition temperature ~200 °C, which decomposes into gas before Al can react (>660 °C). To prepare Al/NC precursor for the Al layer, 240 mg of the solid NC was dissolved in 4 mL DMF. Then 415.5 mg Al was added to the solution and dispersed by sonicating for 30 mins and stirring overnight magnetically. To prepare the AP/NC precursor for the AP layer, 240 mg of the solid NC was dissolved in 4 mL DMF, and then 704.5 mg AP was dissolved into the above solution. Different laminates used the same Al/NC and AP/NC precursors. The absolute mass of NC used in Al and AP layers in different laminates (3 L, 5 L, and 9 L) was the same (240 mg), but the NC mass fraction is different owing to the different mass of Al and AP. Specifically, the NC content in the Al layer is 36.6 wt% while in the AP layer is 25.4 wt%.

2.3. Electrospray deposition

The details of the electrospray can be found in previous studies [40–43]. In a typical electrospray deposition experiment, the feed rates for Al/NC and AP/NC deposition were 1 mL/h and 2 mL/h, respectively, through a needle with an inner diameter of 0.043 mm. A rotating collector covered with aluminum foil was used as a substrate to collect the laminate film. The voltages applied between the needle and substrate for Al/NC and AP/NC were 20 kV and 15 kV, respectively. The jet-to-substrate distance was kept at 4 cm for both cases. This distance was chosen empirically so that the spray was in a stable cone-jet mode and there was enough time for the solvent to evaporate. The total volume of Al/NC and AP/NC precursor sprayed for each film was kept at 1.66 mL, while the thicknesses of each layer were adjusted by varying the duration of the spraying (volume used for each layer). For example, for a three layers (3 L) sandwich laminate, the Al/NC layer uses 1.66 mL of the Al ink while each AP/NC layer uses 0.83 mL of the AP ink. The composition of each ink is shown in Section 2.2. The obtained film was cut into 2 cm × 0.2 cm (length and width) for further combustion tests.

2.4. Characterization

Scanning electron microscopy (SEM, FEI NNS450) operating at 20 kV coupled with energy-dispersive X-ray spectroscopy (EDS) was utilized to analyze the thickness of the laminate films. Thermogravimetric analysis (TG) and differential scanning calorimetry (DSC) was performed on a Netzsch STA 449 F3 Jupiter thermal analyzer with a heating rate of 10 °C/min in argon or oxygen as noted.

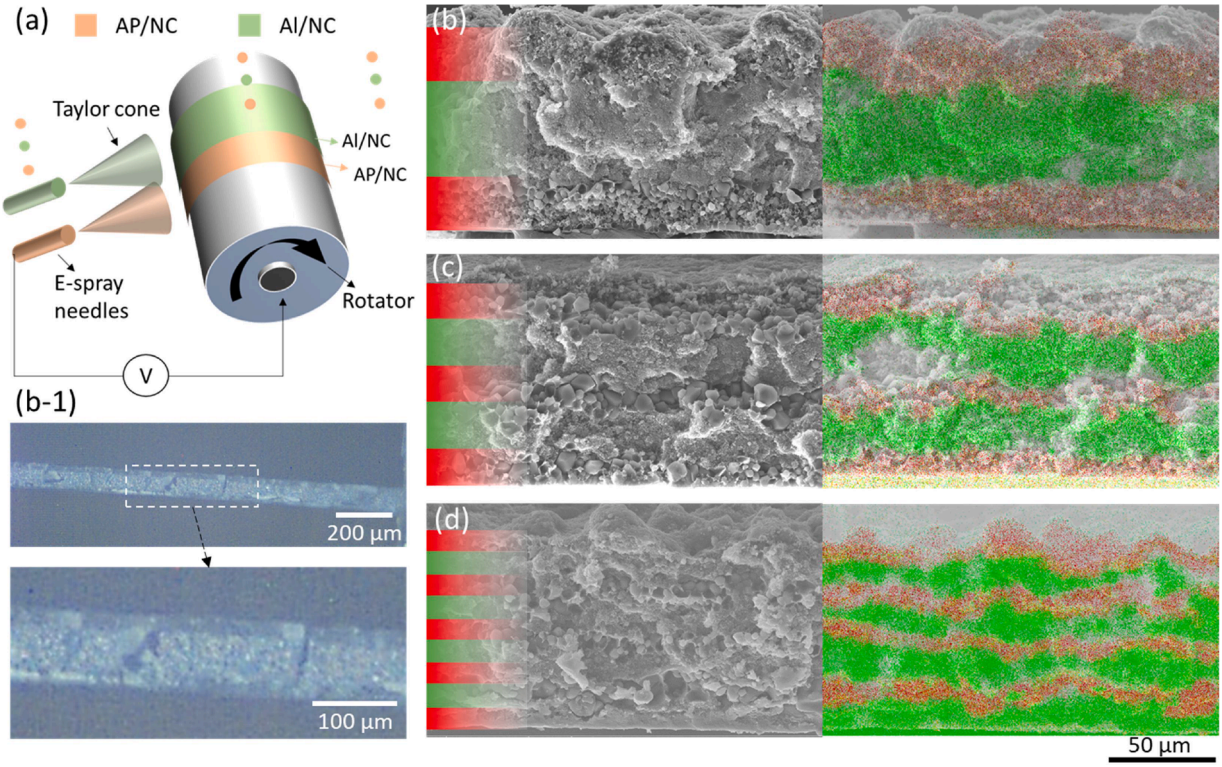

Fig. 3. Schematic showing (a), optical photo (3 layers, b-1), and SEM/EDS images (b-d) of Al/AP sandwich laminates with 3 (b), 5 (c), and 9 (d) layers prepared by E-spraying deposition. The red color represents AP/NC layer and the green color represents Al/NC layer.

Table 1
Thickness of Al and AP layer in different Al/AP sandwich laminates; Note: the total thickness of each film is 95 μm.

Total layers	# of Al layers	# of AP layers	Each Al layer (μm)	Each AP layer (μm)
3L	1	2	45	25
5L	2	3	22	17
9L	4	5	11	10

2.5. Macroscopic and microscopic imaging

The macroscopic and microscopic imaging systems are used in our previous studies [26,27]. The free-standing films were attached to steel support which is mounted to a 3D translational stage and was ignited by nichrome wire (Fig. 2). The whole stage was placed in a chamber (1 L) which would be filled in argon (1 atm) prior to performing the burn test. As Fig. 2 shows, there are two camera systems with different magnifications which can be triggered simultaneously to get two videos for a single event for both macroscopic and microscopic views.

The macroscopic imaging high-speed camera (Vision Research Phantom Miro M110) captures the bottom view at a sample rate of 13,000 frames/s (640×200 pixels) and the microscopic imaging system (Vision Research Phantom VEO710L high-speed camera coupled with Infinity Photo-Optical Model K2 DistaMax) records the top view with a resolution of ~2.2 μm/pixel at a sample rate of 24,000 frames per second). The microscopic imaging system is used to focus a small area of < 1 mm^2, while the macroscopic imaging system is employed to capture the whole film burning with a resolution of ~80 μm/pixel. Microscopic results are used to focus on the Al agglomerates and the flame front, and macroscopic results are employed to get the burn rate and flame temperature.

The flame temperature was estimated with color pyrometry, the details of which can be found in our previous studies [44,45]. Briefly, the intensity of the three-channel Bayer filter (red, green, blue) was extracted to estimate the flame temperature as calibrated with a blackbody source (Mikron M390). The temperature maps were reported after the processing of raw videos using a house-built MATLAB routine. The error threshold for data acceptance and false colorization temperature assignment was set to ~200–300 K. At least triple tests were conducted and the mean value with standard deviation was reported.

3. Results and discussion

3.1. Electrospray deposition of sandwiched AL/AP composite films

As shown in Fig. 3a, the sandwiched Al/AP composite films are prepared by alternative electrospray deposition (Fig. 3a), using a total amount of 30 wt% nitrocellulose (NC) as the binder. The cross-sectional optical and scanning electron microscope (SEM) images of the prepared Al/AP sandwich laminates with different layers (L) of 3, 5, and 9 (3 L, 5 L, and 9 L) prepared are shown in Fig. 3b–d. The total NC, Al, and AP content in different laminates (3 L, 5 L, and 9 L) are fixed at 30 wt%, 26 wt%, and 44 wt%, respectively. The equivalence ratio between Al and AP is approximately 1.

As the cross-sectional SEM/EDS results (Fig. 3b) and larger scale of optical images (Fig. 3b-1) show, one Al layer is sandwiched by two AP layers with a clear interface, rendering the thickness of the layers to be uniform. Three Al/AP sandwich films are fabricated with a fixed total thickness (95 μm) and different bilayer thicknesses, which are shown in Fig. 3b–d and Table 1. The Al layer varies from 11 μm to 45 μm while the thickness of the AP layer varies from 10 μm to 25 μm correspondingly. As Fig. 3c and d show, with the decrease of layer thickness, a more corrugated laminate is observed while the interface between fuel and oxidizer remains clear. AP crystalizes into ~5 μm size particles in different laminates after the electrospraying and causes corrugation of the laminate layers when they approach ~10 μm.

The composition of different Al/AP laminates were confirmed by TG/DSC results (Fig. 4), which shows the composites with different layers a nearly identical decomposition behavior. TGA displays a two-step decomposition, with the first step being the decomposition of NC and the second step being the decomposition of AP, as shown in Fig. 4(a) [46,47,48]. TGA results confirm that the NC content is 30 wt% in different laminates. There are mainly three exothermic peaks and one endothermic peak in DSC (Fig. 4(b)). The first exothermic peak corresponds the decomposition of NC while the second and third peaks are the low temperature decomposition and high temperature decomposition of AP, respectively. The endothermic peak corresponds to the melting of Al. The fact that laminate with different layers has similar TGA/DSC features also indicate that the decomposition of NC and AP are unaffected by the layer thickness.

3.2. In-situ observation of the agglomerating process of Al NPs

The macroscopic and microscopic combustion snapshots of the sandwiched Al/AP laminate are captured by the experimental setup as shown in Fig. 3. Two cameras with different resolutions are used to observe the top and bottom view.

Burn rate of the composite films is obtained from the macroscopic snapshots shown in supporting video 1. The burn rate of the 3-layer Al/AP composite films is 0.5 cm/s, which is 10x lower compared to homogenously mixed energetic films such as Al/AP/PVDF (5 cm/s). From the macroscopic videos, we see the particles ejecting from the

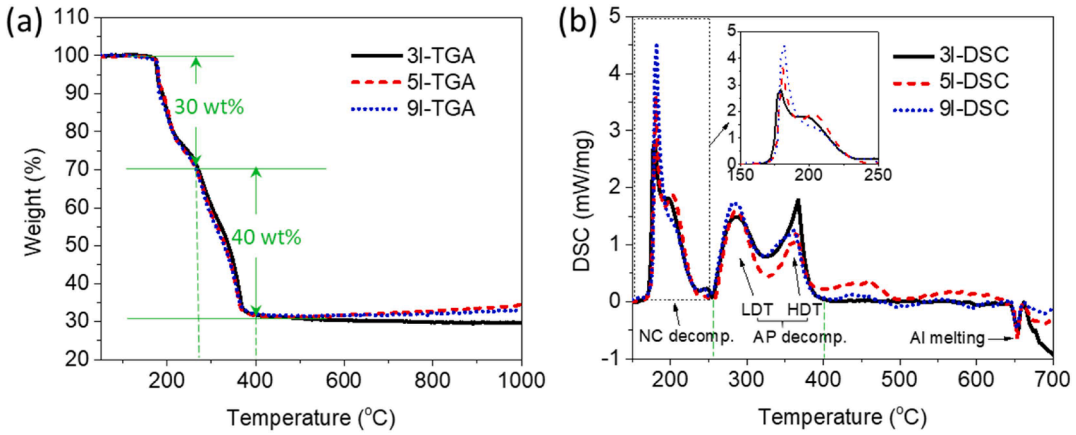

Fig. 4. TGA/DSC results of Al/AP laminates with 3, 5, and 9 layers. The heating rate is 10 °C/min in argon. LDT: low decomposition temperature stage; HDT: high decomposition temperature stage.

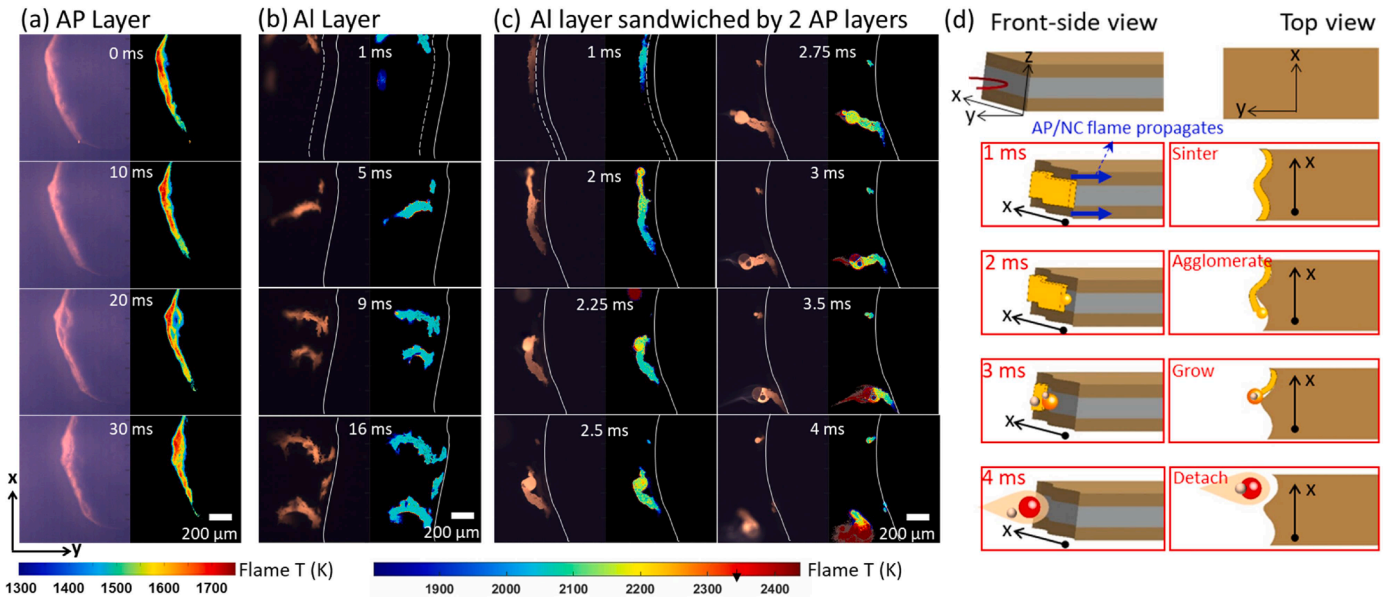

Fig. 5. Top-view microscopic imaging snapshots and their corresponding temperature maps of single AP/NC layer (a), single Al/NC layer (b), and sandwiched Al/AP laminate (c, one Al layer sandwiched by two AP layers); whole process illustration (d) of Al NPs in Al/AP sandwich film. Note: the arrow on the temperature scale refers to the melting point of Al_2O_3 (2345 K). The thickness of the single AP/NC layer (a) and Al/NC layer (b) is 25 μm and 45 μm, respectively, corresponding to the laminate.

burning surface, but the flame front and agglomerating process of Al NPs are barely seen due to their small dimensions. The NC in the film not only serves as a binder, but also serves as an igniter to Al and AP as NC ignites at a relatively low temperature (~200 °C) and releases energy to further decompose AP [46].

The microscopic snapshots demonstrating the combustion process of the single AP (Fig. 5a) and Al layer (Fig. 5b), as well as the sandwiched Al/AP laminate (Fig. 5c) in μm and μs spatial and time resolution are shown in Fig. 5. For the combustion of single layer of AP/NC, the flame is continuously propagating at a speed of 0.44 cm/s, which is close to the propagation rate (0.5 cm/s) of sandwiched Al/AP (3 layers). The measured average flame temperature of AP/NC (~25 wt% NC) at ~1500 K (Fig. 5a) is slightly higher than the adiabatic flame temperature of AP (1400 K), which can be explained by the much faster chemistry than the heat dissipation. For the combustion of single layer of Al/NC (~37 % wt% NC), upon the decomposition and heating of NC (4 kJ/g), a layer of Al aggregates with a thickness of 50–100 μm is heated up to 2000 K (Fig. 5b). As we know Al NPs starts to melt and sinter at its melting point of 933 K, thus at 2000 K, these Al NPs aggregates already melt/sinter and grow to form coral-like structures. It is noted that those coral-like sintered structures are growing in length but do not further coalesce into spheres due to the relatively low temperature (<2000 K). The relatively slow temperature increase at this stage is due to the fact that the intrinsic barrier - Al_2O_3 shell - still remains on the sintering Al (Fig. 5b) as the temperature of the agglomerate at this stage is much lower than the melting point of Al_2O_3 (2345 K) [25]. This highly hinders the further oxidation of Al and prevent the single Al/NC layer from self-propagating.

For Al/AP sandwich structure, similarly, we see that the Al aggregates in the Al layer with a thickness of ~50–100 μm are pre-heated up to 2000 K and the sintering is propagating and extending its length in the x-axis (Fig. 5c, 1ms). Meanwhile the flame from AP/NC provides energy and more importantly oxygen to further oxidize the melting/sintering Al. It is noted that the flame from AP/NC is invisible in Fig. 5c as the aperture and exposure time are tuned for observing much hotter and brighter Al agglomerates, but the flame of AP/NC is confirmed by

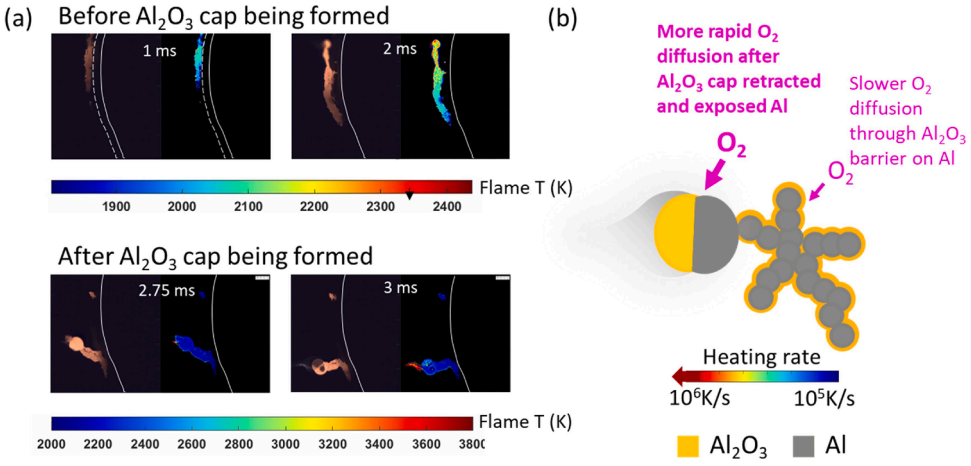

Fig. 6. The pyrometry images (a) and cartoon illustration (b) of different temperature rise before and after Al_2O_3 cap being formed. Note: the 2.75 ms and 3 ms images in (a) were re-calcualted with a larger temperature range due to the saturated temperature of the flume in Fig. 5c.

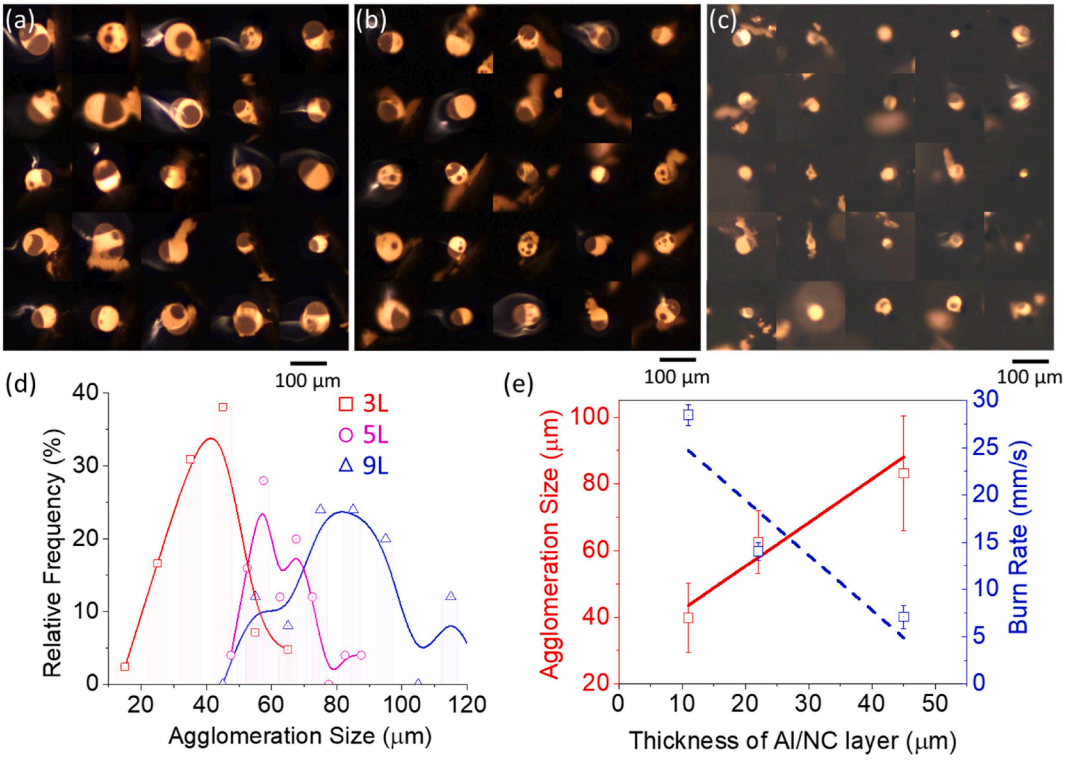

Fig. 7. Typical aluminum coalescing droplets observed by the microscopic imaging system of 3 (a), 5 (b), and 9 (c) layers of Al/AP laminates; Size distribution (d); size and burn rate (e) of the laminates with different Al/NC layer.

imaging the single AP/NC layer as shown in Fig. 5a.

As discussed above, without AP/NC layer, the single Al/NC layer only melts/sinters without further coalescing into a spherical agglomerate owing to the low flame temperature, as evident in Fig. 5b. With the help of energy and oxygen release from AP/NC, the Al/AP sandwich structure (Fig. 5c) has a similar coral-like sintering structure with temperature of 2000 K at the beginning (1 ms), but raises its temperature to 2200–2400 K by forming a spherical agglomerate at the tip of the sintering structure (2 ms). Once the local temperature of the earlier sintering Al aggregates (Fig. 5c, 2ms) approaches the melting point of Al_2O_3 (2345 K), the oxide shells in this hot region collapse and promote the formation of spherical agglomerate – a droplet along with the coalescing of liquid Al inside the shells (Fig. 5c, 2 ms). As shown in Fig. 5c from 1 ms to 2 ms, it takes ~1 ms for the sintering Al aggregates (2000 K) to transform into the first sphere (2300 K) at a rough heating rate of 3 × 10^5 K/s, which continues growing at the tail by coalescing the remaining melted Al and Al_2O_3.

The sphere continues growing (>2 ms) while reacting with the surrounding oxygen, raising the temperature of the droplet above the melting point of Al_2O_3 (2345 K).As displayed in Fig. 5c, around 2.75 ms phase separation occurs between the Al and Al_2O_3, where Al_2O_3 forms a separate phase as a cap (darker area in the main body of agglomerate) on Al droplet due to its surface tension. As the Al_2O_3 retracts into a cap, the Al droplet is exposed directly to the surrounding oxygen, and the oxidation is further accelerated (Fig. 5d). The particle is surrounded by a diffusion flame of Al vapor (3 ms), which indicates the temperature on the interface between Al and O_2 approaches the boiling point of Al (2740 K) [15–17]. The temperature increases from 2400 K to 2700 K takes <0.25 ms at a heating rate >1 × 10^6 K/s, as further illustrated in Fig. 6.

The whole process of Al NPs in Al/AP sandwich film is illustrated in Fig. 5d, from which we divided the process into four stages: (1) sintering of Al aggregates heated by AP/NC flame; (2) Coalescence of Al aggregates when the local temperature is close to the melting point of Al_2O_3; (3) Growing of Al droplet by coalescing, with phase separation between Al and Al_2O_3; (4) Detachment from the burning surface when the coalescence is complete as the temperature is approaching the boiling point of Al.

The dominating factor of Al sintering particularly in the early-stage process, is its temperature, which is controlled by the oxidation of Al with oxidant released from the decomposition of AP/NC. Without an oxidizer, the Al aggregates remain at low temperature and peel off from the burning surface slowly (~20 ms) without transforming into a droplet (Fig. 5b). With an oxidizer, the Al aggregates transform into spherical agglomerates at a heating rate of 10^5 K/s, and the heating rate is further promoted by an order of magnitude to 10^6 K/s when the Al_2O_3 cap is formed and the bare Al is exposed to oxygen environment, as experimentally observed (Fig. 6a) and cartoon illustrated (Fig. 6b).

3.3. Engineering agglomeration size and propagation rate by changing the thickness of sandwiched Al layer

The agglomeration/sintering processes of Al NPs are observed at macroscopic and microscopic scales with different bilayers (3 L, 5 L, and 9 L) of Al/AP sandwich films (See details in supporting video 1). The typical resulting particles formed before detaching the burning surface are temporally imaged, and shown in Fig. 7a–c, for 3 (Fig. 7a), 5 (Fig. 7b), and 9 (Fig. 7c) layers of Al/AP laminates, respectively. The corresponding size distribution is provided in Fig. 7d. The particle size decreases with the increase of the bilayer numbers. That is, with the decrease of the layer thickness of Al/NC in the sandwiched films from 45 μm (3 L) to 11 μm (9 L), the average size reduces from 83 μm to 40 μm or a factor of 9 in particle mass. In contrast, the burn rates of the sandwich films increase from 7 mm/s (3 L) to 28 mm/s (9 L) when the Al/NC layer thinning from 45 μm (3 L) to 11 μm (9 L), as shown in Fig. 7e. It is not surprising that with the reduction of agglomeration size, the burn rate of the Al/AP films increases, as smaller droplets of Al result in a more complete oxidation reaction, providing more heat feedback to the burning surfaces.

As shown in Fig. 7e, the droplet size correlates linearly to the

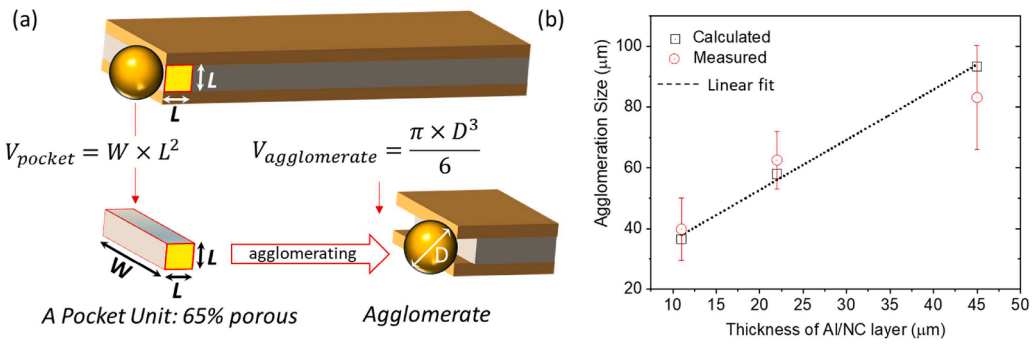

Fig. 8. Calculation process (a) of the droplet size based on the "pocket-size" theory in the Al layer; Calculated and measured drop size changing with the thickness of the Al/NC layer in Al/AP laminates. The width of the film (W) is ~2 mm.

thickness of the Al/NC layer in the sandwiched Al/AP films, which can be explained by a "pocket theory" known in the solid propulsion field. A "pocket" is defined as the volume reserved by the Al NPs that can sinter within the surrounding oxidizers [29,30]. Herein, we construct a simple model of the pocket in the sandwich Al/AP film. As shown in Fig. 8a, the "pocket" of Al NPs is assumed to be a square prism whose size is determined by the width (W) and thickness (L) of the Al/NC layer, which is sandwiched by the oxidizer AP/NC layers. The packing density of Al NPs in the film is estimated at 35 %, owing to how fractal aggregates are known to pack [55]. If assuming all the Al NPs in the pocket turn into one droplet upon melting, the agglomeration size of Al NPs formed within different Al/AP sandwiched laminates can be calculated based on Eq. (1).

The results are shown in Fig. 8b with the combination of the calculated and measured agglomeration size with different Al/NC layer thickness. The calculated size matches well with the experimental data, increasing linearly with the increase of Al/NC thickness, indicating the size is controlled by the sandwiched pocket size of Al NPs within the AP/NC layers. It is notable that the measured agglomerate size for the thickest Al/NC (45 μm) has relatively large deviation compared to thinner films, and measured mean size is smaller than the calculated size. This may be owing to the weaken film upon heating, causing Al agglomerate fall down before it can grow larger across the film (supporting videos).

As we know, the larger the agglomerate, the more percentage of unreacted Al core will exist inside the agglomerate due to imcomplete combustion. In other words, smaller agglomerates will have a more complete combustion of Al compared to larger ones, yielding higher enegry feedback to the unburnt surface and resulting in a higher burn rate. This study reveals that burn rate of a laminate film using Al as the fuel can be manipulated by controlling the agglomeration size via simple manipulation of the layer thickness.

$$V_{pocket} \times 35\% \times Al_{vol\%} \times \rho_{solid\ Al} = V_{agglomerate} \times \rho_{liquid\ Al} \quad (1)$$

Where V_{pocket} is the pocket volume of the refined Al NPs sandwiched by AP/NC layers. 35 % is the packing density of Al NPs in the films. $Al_{vol\%}$ is the volume fraction (25.6 %) of Al in the Al/NC layer. $V_{agglomerate}$ is the final size of the agglomerate and $\rho_{solid\ Al}$ is ~2700 kg/m^3 while $\rho_{liquid\ Al}$ is ~2300 kg/m^3 at 1173 K. The Al_2O_3 shell is not considered in this calculation.

4. Conclusions

In this study, we prepare free-standing microscale sandwich-structured Al/AP laminates to observe the agglomeration/sintering of aluminum nanoparticles (Al NPs) in the presence of ammonium perchlorate (AP). Al/AP laminate sandwich films with a total thickness of ~100 μm and different bilayer thicknesses of Al and AP are prepared by electrospray deposition. The laminate films are characterized by high-speed macroscopic and microscopic imaging systems with pyrometry. We found that the burn rate of the Al/AP sandwich films increases from 7 mm/s to 28 mm/s when the Al layer was reduced from 45 μm (3 L) to 11 μm (9 L), owing to the shorter diffusion distance between fuel and oxidizer. *In-situ* observation of the complete process of the agglomerating of Al NPs shows the stages of agglomeration/sintering, coalescence and growth and final detachment. The relationship between the droplet size and the burn rate is also demonstrated. Simple calculations based on "pocket-theory" support the observed changes in agglomeration size with layer thickness.

Novelty and significance statement

1. Combustion behavior of the laminated films with Al and AP layers is studied with microscopic high-speed videography and pyrometry.
2. Burn rate of the film increases as bilayer thickness decreases due to the reduced diffusion distance between fuel and oxidizer.
3. A complete process of agglomeration/sintering, coalescence, growth, and final detachment of Al particles is observed *in-situ*.
4. A correlation between agglomeration size and bilayer thickness is demonstrated.
5. The observed agglomeration size is consistent with theoretical predication from layer thickness based on "pocket-theory".

CRediT authorship contribution statement

Haiyang Wang: Conceptualization, Data curation, Formal analysis, Methodology, Writing – original draft. **Yujie Wang:** Conceptualization, Data curation, Formal analysis, Methodology, Writing – original draft. **Michael R. Zachariah:** Supervision, Investigation, Funding acquisition, Validation, Writing – review & editing.

Declaration of Competing Interest

On behalf of all the authors, we declare no conflict of interest. This work is original and has not been considered for publication elsewhere.

Acknowledgments

We gratefully acknowledge support from AFOSR. We also thank the CFAMM at the University of California, Riverside, for their microscopy support. We thank Prithwish Biswas for helpful discussions on the manuscript.

Supplementary materials

Supplementary material associated with this article can be found, in the online version, at doi:10.1016/j.combustflame.2023.113117.

References

[1] R.A. Yetter, Progress towards nanoengineered energetic materials, Proc. Combust. Inst. 38 (2021) 57–81.
[2] E.L. Dreizin, Metal-based reactive nanomaterials, Prog. Energy Combust. Sci. 35 (2009) 141–167.
[3] L.T. DeLuca, Overview of Al-based nanoenergetic ingredients for solid rocket propulsion, Def. Technol. 14 (2018) 357–365.
[4] X. Ma, Y. Li, I. Hussain, R. Shen, G. Yang, K. Zhang, Core–shell structured nanoenergetic materials: preparation and fundamental properties, Adv. Mater. 32 (2020), 2001291.
[5] J. Hübner, M. Klaumünzer, M. Comet, C. Martin, L. Vidal, M. Schäfer, C. Kryschi, D. Spitzer, Insights into combustion mechanisms of variable aluminum-based iron oxide/-hydroxide nanothermites, Combust. Flame 184 (2017) 186–194.
[6] Y. Sami, N. Richard, D. Gauchard, A. Estève, C. Rossi, Selecting machine learning models to support the design of Al/CuO nanothermites, J. Phys. Chem. A. 126 (2022) 1245–1254.
[7] D. Sundaram, V. Yang, R.A. Yetter, Metal-based nanoenergetic materials: synthesis, properties, and applications, Prog. Energy Combust. Sci. 61 (2017) 293–365.
[8] M. Comet, C. Martin, F. Schnell, D. Spitzer, Nanothermites: a short review. Factsheet for experimenters, present and future challenges, Propell. Explos. Pyrotech. 44 (2019) 18–36.
[9] J.J. Granier, M.L. Pantoya, Laser ignition of nanocomposite thermites, Combust. Flame 138 (2004) 373–383.
[10] L. Meda, G. Marra, L. Galfetti, F. Severini, L. De Luca, Nano-aluminum as energetic material for rocket propellants, Mater. Sci. Eng. C. 27 (2007) 1393–1396.
[11] J. Zhi, L. Shu-Fen, Z. Feng-Qi, L. Zi-Ru, Y. Cui-Mei, L. Yang, L. Shang-Wen, Research on the combustion properties of propellants with low content of nano metal powders, Propell. Explos. Pyrotech. 31 (2006) 139–147.
[12] L. Galfetti, L.T. DeLuca, F. Severini, G. Colombo, L. Meda, G. Marra, Pre and post-burning analysis of nano-aluminized solid rocket propellants, Aerosp. Sci. Technol. 11 (2007) 26–32.
[13] E.A. Lebedeva, I.L. Tutubalina, V.A. Val'tsifer, V.N. Strel'nikov, S.A. Astaf'eva, I. V. Beketov, Agglomeration of the condensed phase of energetic condensed systems containing modified aluminum, Combust. Explos. Shock Waves 48 (2012) 694–698.
[14] P. Chakraborty, M.R. Zachariah, Do nanoenergetic particles remain nano-sized during combustion? Combust. Flame 161 (2014) 1408–1416.
[15] W. Ao, X. Liu, H. Rezaiguia, H. Liu, Z. Wang, P. Liu, Aluminum agglomeration involving the second mergence of agglomerates on the solid propellants burning surface: experiments and modeling, Acta Astronaut. 136 (2017) 219–229.
[16] Y. Chen, D.R. Guildenbecher, K.N.G. Hoffmeister, M.A. Cooper, H.L. Stauffacher, M.S. Oliver, E.B. Washburn, Study of aluminum particle combustion in solid propellant plumes using digital in-line holography and imaging pyrometry, Combust. Flame 182 (2017) 225–237.
[17] B. Jin, Z. Wang, G. Xu, W. Ao, P. Liu, Three-dimensional spatial distributions of agglomerated particles on and near the burning surface of aluminized solid propellant using morphological digital in-line holography, Aerosp. Sci. Technol. 106 (2020), 106066.
[18] L. Li, X. Chen, C. Zhou, W. Li, M. Zhu, Experimental and model investigation on agglomeration of aluminized fuel-rich propellant in solid fuel ramjet, Combust. Flame 219 (2020) 437–448.
[19] W. Ao, P. Liu, H. Liu, S. Wu, B. Tao, X. Huang, L.K.B. Li, Tuning the agglomeration and combustion characteristics of aluminized propellants via a new functionalized fluoropolymer, Chem. Eng. J. 382 (2020), 122987.
[20] E.R. Wainwright, S.V. Lakshman, A.F.T. Leong, A.H. Kinsey, J.D. Gibbins, S. Q. Arlington, T. Sun, K. Fezzaa, T.C. Hufnagel, T.P. Weihs, Viewing internal bubbling and microexplosions in combusting metal particles via x-ray phase contrast imaging, Combust. Flame 199 (2019) 194–203.
[21] M.D. Grapes, R.V. Reeves, K. Fezzaa, T. Sun, J.M. Densmore, K.T. Sullivan, In situ observations of reacting Al/Fe2O3 thermite: relating dynamic particle size to macroscopic burn time, Combust. Flame 201 (2019) 252–263.
[22] A.R. Demko, K.J. Hill, E.K. Ismael, A. Kastengren, Observation of aluminum interaction with the binder melt layer using high-speed synchrotron-based phase contrast imaging, Combust. Flame 241 (2022), 112054.
[23] H. Wang, B. Julien, D. Kline, Z. Alibay, M. Rehwoldt, C. Rossi, M. Zachariah, Probing the Reaction Zone of Nanolaminates at ~μs Time and ~μm Spatial Resolution, J. Phys. Chem. C 124 (2020) 13679–13687.
[24] H. Wang, D.J. Kline, M.R. Zachariah, In-operando high-speed microscopy and thermometry of reaction propagation and sintering in a nanocomposite, Nat. Commun. 10 (2019) 3032.
[25] Y. Wang, E. Hagen, P. Biswas, H. Wang, M.R. Zachariah, Imaging the combustion characteristics of Al, B, and Ti composites, Combust. Flame 252 (2023), 112747.
[26] H. Wang, D.J. Kline, P. Biswas, M.R. Zachariah, Connecting agglomeration and burn rate in a thermite reaction: role of oxidizer morphology, Combust. Flame 231 (2021), 111492.
[27] H. Wang, D.J. Kline, M.C. Rehwoldt, M.R. Zachariah, Carbon fibers enhance the propagation of high loading nanothermites: in situ observation of microscopic combustion, ACS Appl. Mater. Interfaces (2021).
[28] H. Wang, P. Biswas, D.J. Kline, M.R. Zachariah, Flame stand-off effects on propagation of 3D printed 94 wt% nanosized pyrolants loading composites, Chem. Eng. J. 434 (2022), 134487.
[29] S.R. Chakravarthy, J.M. Seitzman, E.W. Price, R.K. Sigman, Intermittent burning of ammonium perchlorate-hydrocarbon binder monomodal matrixes, sandwiches, and propellants, J. Propuls. Power. 20 (2004) 101–109.
[30] M. Navaneethan, V. Srinivas, S.R. Chakravarthy, Coupling of leading edge flames in the combustion zone of composite solid propellants, Combust. Flame 153 (2008) 574–592.
[31] T. Gaduparthi, M. Pandey, S.R. Chakravarthy, Gas phase flame structure of solid propellant sandwiches with different reaction mechanisms, Combust. Flame 164 (2016) 10–21.
[32] E.W. Price, Effect of multidimensional flamelets in composite propellant combustion, J. Propuls. Power. 11 (1995) 717–729.
[33] C. Vijay, P.A. Ramakrishna, Estimation of burning characteristics of AP/HTPB composite solid propellant using a sandwich model, Combust. Flame 217 (2020) 321–330.
[34] G. Xu, P. Liu, W. Ao, B. Jin, Theoretical study of the flame describing function of AP/HTPB propellant flame based on sandwich model, Acta Astronaut. 162 (2019) 207–215.
[35] K. Gnanaprakash, S.R. Chakravarthy, Effect of curing agent on the plateau burning mechanism of solid propellant sandwiches, J. Propuls. Power 34 (2018) 1442–1454.
[36] K. Gnanaprakash, S.R. Chakravarthy, R. Sarathi, Combustion mechanism of composite solid propellant sandwiches containing nano-aluminium, Combust. Flame 182 (2017) 64–75.
[37] H. Wang, G. Jian, W. Zhou, J.B. DeLisio, V.T. Lee, M.R. Zachariah, Metal iodate-based energetic composites and their combustion and biocidal performance, ACS Appl. Mater. Interfaces 7 (2015) 17363–17370.
[38] H. Wang, G. Jian, G.C. Egan, M.R. Zachariah, Assembly and reactive properties of Al/CuO based nanothermite microparticles, Combust. Flame 161 (2014) 2203–2208.
[39] H. Wang, J.B. DeLisio, G. Jian, W. Zhou, M.R. Zachariah, Electrospray formation and combustion characteristics of iodine-containing Al/CuO nanothermite microparticles, Combust. Flame 162 (2015) 2823–2829.
[40] X. Li, P. Guerieri, W. Zhou, C. Huang, M.R. Zachariah, Direct deposit laminate nanocomposites with enhanced propellent properties, ACS Appl. Mater. Interfaces. 7 (2015) 9103–9109.
[41] R.J. Jacob, D.J. Kline, M.R. Zachariah, High speed 2-dimensional temperature measurements of nanothermite composites: probing thermal vs. gas generation effects, J. Appl. Phys. 123 (2018), 115902.
[42] D.J. Kline, M.C. Rehwoldt, J.B. DeLisio, S.C. Barron, H. Wang, Z. Alibay, J. C. Rodriguez, G.M. Fritz, M.R. Zachariah, In-operando thermophysical properties and kinetics measurements of Al-Zr-C composites, Combust. Flame 228 (2021) 250–258.
[43] H. Wang, D.J. Kline, M. Rehwoldt, T. Wu, W. Zhao, X. Wang, M.R. Zachariah, Architecture can significantly alter the energy release rate from nanocomposite energetics, ACS Appl. Polym. Mater. 1 (2019) 982–989.
[44] C. Dennis, B. Bojko, On the combustion of heterogeneous AP/HTPB composite propellants: a review, Fuel 254 (2019), 115646.
[45] N.S. Cohen, A pocket model for aluminum agglomeration in composite propellants, AIAA J. 21 (1983) 720–725.
[46] F. Maggi, L.T. DeLuca, A. Bandera, Pocket model for aluminum agglomeration based on propellant microstructure, AIAA J. 53 (2015) 3395–3403.
[47] J.K. Sambamurthi, E.W. Price, R.K. Sigman, Aluminum agglomeration in solid-propellant combustion, AIAA J. 22 (1984) 1132–1138.
[48] C.D. Zangmeister, J.G. Radney, L.T. Dockery, J.T. Young, X. Ma, R. You, M. R. Zachariah, Packing density of rigid aggregates is independent of scale, Proc. Natl. Acad. Sci. 111 (2014) 9037–9041.